Detoxification of Lignocellulosic Hydrolysates by *in situ* Formation of Fe(0) Nanoparticles on Activated Carbon

Mohd Shaiful Sajab,[a,b,*] Jude Santanaraj,[a,b] Abdul Wahab Mohammad,[a,b] Hatika Kaco,[c] and Shuhaida Harun [a,b]

The breakdown of lignocellulosic biomass into fine chemicals is an essential subsequence process of bioconversion technology. However, the manner of decomposition can contribute significantly to inefficiency of the overall conversion. Certain low molecular weight byproducts of the lignin and hemicellulose within lignocellulosic hydrolysate are toxic, making it necessary to carry out a complicated detoxification process. In this study, detoxification of hydrolysate was performed by the adsorption and catalytic oxidation, as well as the integration of both techniques on the targeted compounds of acid-soluble lignin (ASL) and synthetic furfural. In spite of the high selectivity of its adsorption and catalytic oxidation, by relying on just these techniques, the hydrolysate was unable to completely remove ASL and furfural. However, by depositing Fe(0) nanoparticles on the surface active sites of the adsorbent, the integration of the adsorption-oxidation technique provided sufficient performance in the removal of ASL and furfural.

Keywords: ASL; Fenton oxidation; Furfural; Lignocellulosic; Zero valent iron

Contact information: a: Research Center for Sustainable Process Technology (CESPRO), Faculty of Engineering and Built Environment, Universiti Kebangsaan Malaysia, 43600 Bangi, Selangor, Malaysia; b: Department of Chemical and Process Engineering, Faculty of Engineering and Built Environment, Universiti Kebangsaan Malaysia, 43600 Bangi, Selangor, Malaysia; c: Kolej GENIUS Insan, Universiti Sains Islam Malaysia, Bandar Baru Nilai, 71800, Nilai, Negeri Sembilan, Malaysia;
** Corresponding author: mohdshaiful@ukm.edu.my*

INTRODUCTION

The bioconversion of agricultural waste has the potential to replace the majority of non-renewable resources and their products, particularly those of petroleum-based derived chemicals (Chaturvedi and Verma 2013). There are several stages in the bioconversion of lignocelluloses, namely pretreatment, hydrolysis, and fermentation (Chin *et al*. 2013). The breakdown of cellulose and hemicellulose into simple sugars constitutes the most essential stage in bioconversion (Qureshi and Manderson 1995; Chin *et al*. 2016; Sambusiti *et al*. 2016). However, in the subsequent stages, the presence of lignin and hemicellulose derivatives (such as furfural, hydroxymethylfurfural, acetic acid, phenolic compounds, *etc*.) prevent the penetration of chemicals to the glucose-xylose and affect the physiology and viability of the cell for bioconversion process, thereby hindering the sugar conversion process (Soleimani *et al*. 2015; Jönsson and Martín 2016). Thus, in order to maximize the sugar conversion yield, lignocellulosic hydrolysates require post-treatment in the form of detoxification and removal of inhibitors.

The detoxification of lignocellulosic hydrolysate includes chemical additives, enzymatic treatment, heating, and vaporization, liquid-liquid extraction, liquid-solid extraction, and microbial treatment (Sambusiti *et al*. 2016). The adsorptive process enhances the interactivity and efficiency of the removal of specific organic matter. The operational cost and post-regeneration inefficiency of commercially activated carbon are unfavorable aspects of hydrolysate detoxification. Therefore, it is necessary to design adsorbents with specific and innovative functions for the removal of hydrolysate inhibitors.

Oxidative pre-treatment has high selectivity towards the lignin of lignocellulosic biomass (Gould 1985; Mishima *et al*. 2006; Santanaraj *et al*. 2017). In this method, iron-based Fenton's reagents, which are involved in the generation of free hydroxyl radicals, are important; these radicals react with the surrounding organic matter and degrade them into smaller carbonaceous compounds (Minella *et al*. 2014). The various types of Fenton's reagents can be distinguished by their reactivity and free hydroxyl radical generation capacities (Pereira *et al*. 2012). Unlike other iron-based reagents, nanoscale zero-valent iron [Fe(0)] has immense potential owing to its efficient reactivity with a wide scope of contaminants during water remediation (Sun *et al*. 2006; Phenrat and Saleh 2007; Geng *et al*. 2009; Yan *et al*. 2010; Rosická and Sembera 2011; Zhang *et al*. 2013; Torrey *et al*. 2015; Santos *et al*. 2017; Oruç *et al*. 2019; Sajab *et al*. 2019).

In this study, a combination of adsorption and Fenton oxidation has been utilized for the detoxification of lignocellulosic hydrolysate through the removal of acid-soluble lignin (ASL) and synthetic furfural. The adsorption and oxidation techniques were optimized separately and later integrated as per the results of adsorption and degradation studies. Moreover, the *in situ* generation of Fe(0) was exploited to enhance the degradation of lignocellulose.

EXPERIMENTAL

Materials

Commercial activated carbon (AC) (synthesized from coconut shells) of particle size 0.42 mm to 1.70 mm were obtained from Concepts Ecotech Sdn. Bhd., Kuala Langat, Malaysia. Oil palm empty fruit bunch (EFB) fibers of size 106 µm to 150 µm were procured from Szetech Engineering Sdn. Bhd., Shah Alam, Malaysia. Iron(III) chloride hexahydrate, sodium hydroxide, 30% hydrogen peroxide, 32% hydrochloric acid, and sodium borohydride were purchased from Merck (New Jersey, United States) and used for the preparation of Fenton's reagent. GR-grade synthetic furfural (Merck) was used without further purification. To prepare acid-soluble lignin (ASL), the oil palm EFB fibers were dissolved in 72% H_2SO_4 (Merck) in a ratio of 1 g to 15 mL at 10 °C in a water bath shaker for 1 h. Subsequently, the concentration of the H_2SO_4 solution was reduced from 72% to 4% *via* the addition of deionized (DI) water. The mixture was autoclaved at 121 °C for 1 h, cooled at room temperature, and vacuum-filtered to yield an ASL solution.

Fe(0) Nanoparticles Preparation

An 8 mg/L stock solution of Fe(III) was prepared by dissolving $FeCl_3$ in DI water with the addition of fractional drops of 1 M HCl to prevent sedimentation. Colloidal Fe(0) was prepared from iron and a reducing agent ($NaBH_4$ in 100 mL of ethanol) in a 1:2 weight ratio with the addition of a stabilizer (ethylenediaminetetraacetic acid, EDTA). The

resulting Fe(0) was separated by centrifugation at 10,000 revolutions per minute (rpm) for 15 min, after which it was washed and sonicated in deionized water for 1 h to remove the excess ethanol. The sample was then kept dry until further use. The *in situ* synthesis of Fe(0) on AC was performed by adsorbing 8 mg/L of Fe(III) onto the $NaBH_4$ in the aforementioned ratio.

Adsorption-oxidation

With regards to the preliminary study, the adsorption capacity of AC was determined by adding 0.1 g of AC to 50 mL of adsorbate solution at 200 rpm for 4 h at room temperature. At specific time intervals, an aliquot of the sample was taken for dilution, after which the concentrations of ASL and furfural were measured using a UV-Vis spectrophotometer. As for the isotherm study, 0.1 g of AC was mixed with 50 mL of the adsorbate solution and placed in a water bath shaker at 200 rpm for 4 h at room temperature and atmospheric pressure. The final concentration was measured and analysed according to the following Eqs. 1 and 2,

$$q_t = \frac{(C_0 - C_t)V}{m} \quad (1)$$

$$\% \text{ of adsorbate removal} = \frac{(C_0 - C_t)}{C_0} \times 100\% \quad (2)$$

where C_0, C_t, and C_e are the initial concentration, the concentration of adsorbate at the time *t*, and the concentration at the equilibrium (mg/L), while *m* and *V* are the mass of the AC (g) and the volume of the adsorbate solution (L).

The removal of the ASL and furfural via Fenton's oxidation involved the use of different Fenton reagents [Fe(III) and Fe(0)] with the aid of 200 mmol of H_2O_2. This experiment was performed under conditions that were similar to that of adsorption, i.e. 8 mg/L of AC in 50 mL of adsorbate over a reaction time of 4 h. Meanwhile, simultaneous adsorption-Fenton oxidation generated Fenton reagents, Fe(III) and Fe(0), on commercial AC in a ratio of 0.1 g of AC to 8 mg/L of the Fenton reagent. In this process, Fe(III) was formed in the presence of 200 mmol of H_2O_2. The initial and final concentrations of ASL and furfural were measured accordingly using a UV-Vis spectrophotometer.

Characterization

The surface morphology of Fe(0) was determined via transmission electron microscopy (TEM) (CM 12 Philips, Eindhoven, Netherlands). Meanwhile, the structural changes in AC with Fe(III) and Fe(0) deposits were identified by field emission scanning electron microscopy (FESEM) (Merlin Compact, Zeiss Pvt. Ltd., Oberkochen, Germany). X-ray diffractometry (XRD) was performed to verify the changes in the crystalline structure of AC (Bruker D8 Advanced, Bruker, Billerica, MA, USA). Subsequently, the zeta potential and diameter of diluted Fe(0) were evaluated using a Malvern Zetasizer (City, UK). The concentrations of ASL and furfural were monitored via UV-Vis spectrophotometry, whereby the maximum wavenumbers, λ_{max}, were calibrated according to the Lambert-Beer law of linearity at 205 nm and 275 nm, respectively (Single Beam UV Spectrophotometer SP-UV 300SRB, Spectrum Instruments GmbH, Überlingen, Germany).

RESULTS AND DISCUSSION

Characterization

As per the morphological analysis, the spherical particles of synthesized Fe(0) were clearly visible in the TEM micrograph (Fig. 1a). Additionally, the partial Fe(0) particles appeared to be aggregated into a chain-like structure. The diameters of the individual particles were 41.7 nm to 42.5 nm, which corresponded to those of previous studies (Sun *et al*. 2006; Yan *et al*. 2010; Zhang *et al*. 2013; Santos *et al*. 2017). Even though the agglomeration of Fe(0) was temporary (owing to its magnetic property), the mobility of the particles was restricted in this phase (Sun *et al*. 2006; Phenrat and Saleh 2007; Rosická and Sembera 2011). In the depths of the Fe(0) micrograph, the oxidative phases of iron were clearly observed in the form of different color tones; darker tones in the Fe(0) core represented those of larger atomic numbers, while the lighter tones indicated the formation of iron oxides (Sun *et al*. 2006). Since Fe(0) is highly reactive, the oxidized layer on its surface kept expanding, owing to its transformation into FeOOH. Besides, the reactivity of Fe(0) with an aqueous medium led to the expeditious formation of larger Fe(0) particles (Torrey *et al*. 2015).

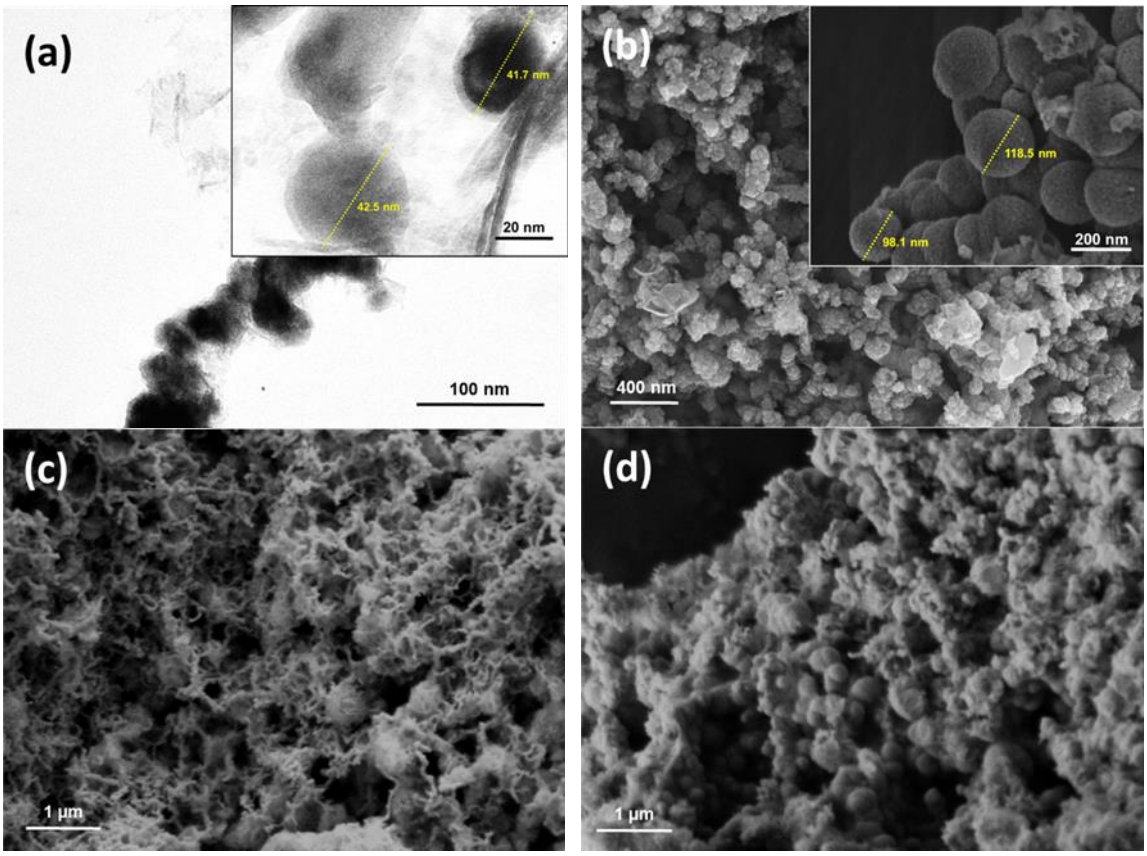

Fig. 1. Morphological structure of: (a) Fe(0) by TEM micrograph image; (b) Fe(0) by FESEM micrograph image; (c) AC with deposited Fe(III); (d) AC with deposited Fe(0)

Given the significant increase in diameter (in the range of 98.1 nm to 118.5 nm), the expanded Fe(0) particles were clearly visible in the FESEM image [Fig. 1(b)]. The surface morphologies of the Fe(III) and Fe(0) deposited on the AC are displayed in Fig.

1(c) and Fig. 1(d). Evidently, the presence of Fe(III) on the surface of AC was insignificant, since the macropores on the outer surface AC had diameters of about 10 nm to 50 nm and consisted of electron-free areas when compared with the entire carbon matrix (Onganer and Temur 1998). In contrast, the spherical particles of Fe(0) was clearly observed on the surface of AC with a decent distribution.

The crystallograph of AC was observed in the XRD pattern (Fig. 2a). Neat AC was identified by the presence of two obvious peaks [(002) and (101)] at 2θ = 23° and 44°, respectively, which denoted the characteristics of graphite crystals (Dantas *et al*. 2006). However, an individual analysis of Fe(0) yielded significant peaks at 44°, which corresponded to the (110) plane (Zhang *et al*. 2013). It was difficult to identify the phase difference between neat AC and deposited Fe(0), since peak (101) overlapped peak (110) (Geng *et al*. 2009). Meanwhile, the diameters, as measured by a zetasizer (Fig. 2b) contained two significant peaks at 94.3 nm (38.5% intensity) and 264.7 nm (61.5% intensity). Specifically, the dispersed nanoparticles were less than 100 nm in size and had an aggregated chain-like structure, as shown in Fig. 1(a). Despite the broad distribution of the particle sizes, Fe(0) had an average zeta potential of -7.2 mV (Sun *et al*. 2006; Saad *et al*. 2019).

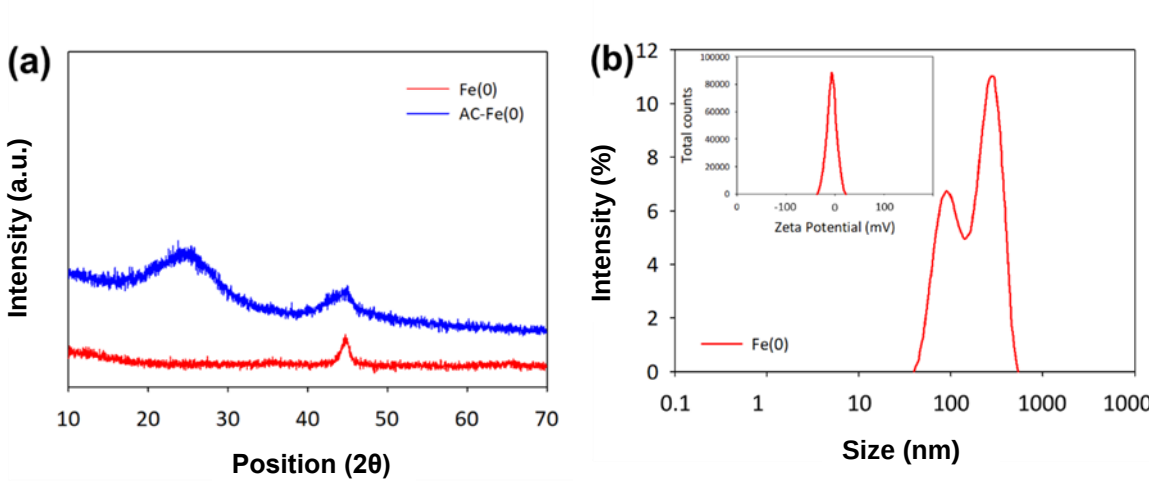

Fig. 2. Characterization of (a) Fe(0) particles and AC with deposited Fe(0) on XRD analysis; (b) zeta size and potential of Fe(0)

Adsorption Efficiency

The efficiencies of ASL and furfural uptake by the neat AC have been analyzed in terms of adsorption kinetics. With reference to Fig. 3(a), 15.3% and 27.4% of the ASL and furfural were adsorbed onto 0.1 g of the AC within 4 h. Evidently, the adsorption of ASL and furfural was facilitated by the porous microstructure of AC and the broad spectrum of the functional groups on its surface (Sambusiti *et al*. 2016). Also, the rates of adsorption of the ASL and furfural attained an equilibrium within 50 min and 120 min. The difference in the molecular weights of ASL and furfural in the dissolved solution were likely attributable to the penetration of particles through the pores of AC. On another matter, the addition of Fe(III) led to slight reductions in the degradation of ASL (12.7% removal) and furfural (26.3% removal). Even though AC possessed distinct surface-active sites, the specific uptake of Fe(III) deposited on the AC reduced the latter's interaction with ASL and furfural (Mopoung *et al*. 2015). While the maximum uptake of the adsorbate can be

quantitatively measured using adsorption isotherm models, it is difficult to determine precisely the concentration of ASL *via* an indirect analytical method such as UV-spectrophotometry.

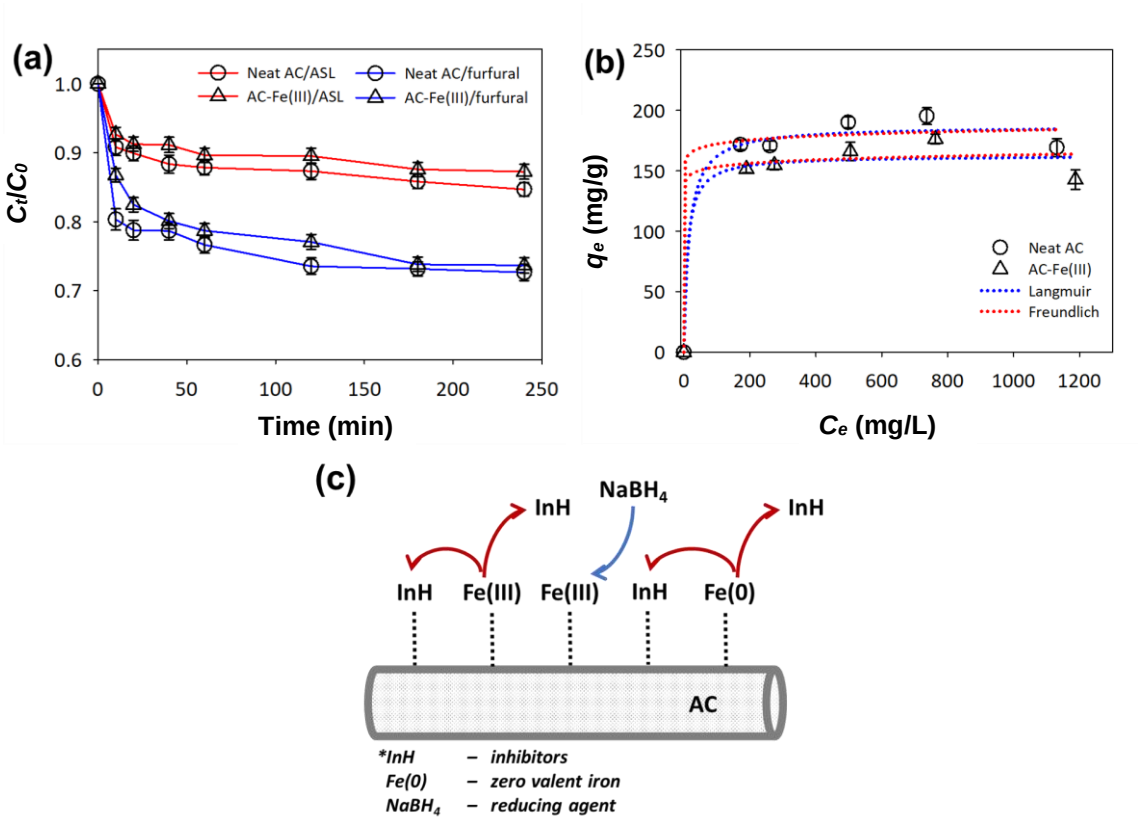

Fig. 3. Adsorption kinetics of: (a) ASL and furfural uptake for 4 h; (b) the non-linearized isotherm adsorption of Langmuir and Freundlich of furfural and (c) schematic diagram of adsorption-oxidation behavior (adsorbent: 0.1 g; pH: 5; ASL: 100%, furfural: 500 mg/L to 1500 mg/L)

The adsorption isotherm was only determined for furfural uptake. This was followed by the use of Langmuir and Freundlich models – as per Eq. 3 and 4 (Freundlich 1907; Langmuir 1917),

$$q_e = \frac{Q_0 b C_e}{1+bC_e} \quad (3)$$

$$q_e = K_F C_e^{1/n_F} \quad (4)$$

where Langmuir isotherm expressed, Q_0 is the maximum adsorption capacity of furfural per unit mass of adsorbent (mg/g), and b is a constant related to the adsorption energy (L/mg). In the Freundlich isotherm, K_F and $1/n_F$ are the constants, where K_F is the relative adsorption capacity of the adsorbent and n_F is the degree of the dependence of adsorption on the equilibrium concentration of the furfural. Figure 3(b) shows the correlation between the prediction and experimental of furfural adsorption; Table 1 shows the summary of the computed data. Accordingly, the larger coefficient of correlation for the Langmuir isotherm suggests the involvement of monolayer interactions between the furfural and AC. In addition, the maximum uptake of furfural by neat AC was higher than that by the AC-

Fe(III) (Q_0 = 186.9 and 162.6 mg/g, respectively) even though their adsorption kinetics were similar. However, due to the fact that the uptake of Fe(III) ions took place in the surface site of the activated carbon as shown in the schematic diagram [see Fig. 3(c)], the adsorption capacity of activated for the inhibitors uptake was reduced significantly.

Table 1. Calculated Langmuir and Freundlich Isotherm Constants for the Uptake of Furfural on Neat AC and Deposited Fe(III) on AC

Adsorbate	Langmuir			Freundlich		
	Q_0	b	R^2	K_F	n	R^2
Neat AC	186.9	0.064	0.997	36.58	9.39	0.980
AC-Fe(III)	162.6	0.009	0.970	37.41	8.73	0.967

Note: Q_0 (mg/g) = maximum adsorption capacity; b (L/mg) = constant related to adsorption the adsorption energy; K_F ((mg/g)(L/mg)$^{1/n}$) = relative adsorption capacity; n = degree of dependence of adsorption; R^2 = coefficient of determination. Adsorbent: 0.1 g; pH: 5; furfural: 500 mg/L to 1500 mg/L.

Degradation Kinetics of Adsorption-oxidation

Figure 4(a) and Fig. 4(b) show the degradation kinetics of ASL and furfural, respectively, during adsorption, catalytic oxidation, and adsorption-oxidation. In the graphs, neat AC and Fe(III)/FOx were used as a reference for the individual reactions of adsorption and Fenton oxidation. Based on the efficiency of adsorption in Fig. 3, the extent of oxidative removal of ASL and furfural in the presence of 200 mmol of H_2O_2 were 26.4% and 35.8%, respectively. Basically, the presence of Fe(III) in solution catalyzed the oxidative process by increasing the production of hydroxyl radicals, which facilitated the degradation of ASL and furfural (Dantas *et al*. 2006). Nevertheless, the rates of removal of ASL and furfural reached a saturation limit 2 h into the process. Presumably this was due to the inversion of the oxidation reaction (*i.e.* from Eq. 6 to Eq. 5), which led to a decline in the availability of Fe^{2+} (Santanaraj *et al*. 2017). Accordingly, the reduction in Fe^{2+} led to a decrease in the production of hydroxyl radicals, which in turn, slowed down the ASL removal rate (Suh *et al*. 2003). Equation 5 to 10 exhibit the possible process reactions that could occur in Fenton oxidation until the degradation of the organic compounds (R in Eq. 10 represents ASL and furfural) (Zhang *et al*. 2014).

$$Fe^0 + O_2 + 2H^+ \rightarrow Fe^{2+} + H_2O_2 \quad (4)$$

$$Fe^{3+} + H_2O_2 \rightarrow Fe^{2+} + H^+ + HO_2^{\bullet} \quad (5)$$

$$Fe^{2+} + H_2O_2 \rightarrow Fe^{3+} + {}^{\bullet}OH^{+} + OH^{-} \quad (6)$$

$$^{\bullet}OH + Fe^{2+} \rightarrow Fe^{3+} + OH^{-} \quad (7)$$

$$HO_2^{\bullet} + Fe^{2+} + H^+ \rightarrow Fe^{3+} + H_2O_2 \quad (8)$$

$$HO_2^{\bullet} + Fe^{3+} \rightarrow Fe^{2+} + H^+ + O_2 \quad (9)$$

$$RH + {}^{\bullet}OH \rightarrow R^{\bullet} + H_2O \quad (10)$$

In the adsorption-oxidation reaction, the rates of removal of ASL and furfural via deposition of Fe(III) on AC [AC-Fe(III)/FOx] increased significantly. By 4 h into the reaction, AC-Fe(III)/FOx efficiently removed 57.8% of the ASL; this figure was twice that

of neat AC-Fe(III). Similarly, AC-Fe(0)/Fe(III) removed up to 70.2% of the furfural. Unlike the single reaction between neat AC and Fe(III), AC-Fe(III)/FOx could have provided an AC surface of greater reactivity. Because the for-adsorption surfaces were able to immobilize both Fe(III) and ASL/furfural, the hydroxyl radicals generated by Fe(III) immediately reacted with the target organic compounds (Shi *et al*. 2017).

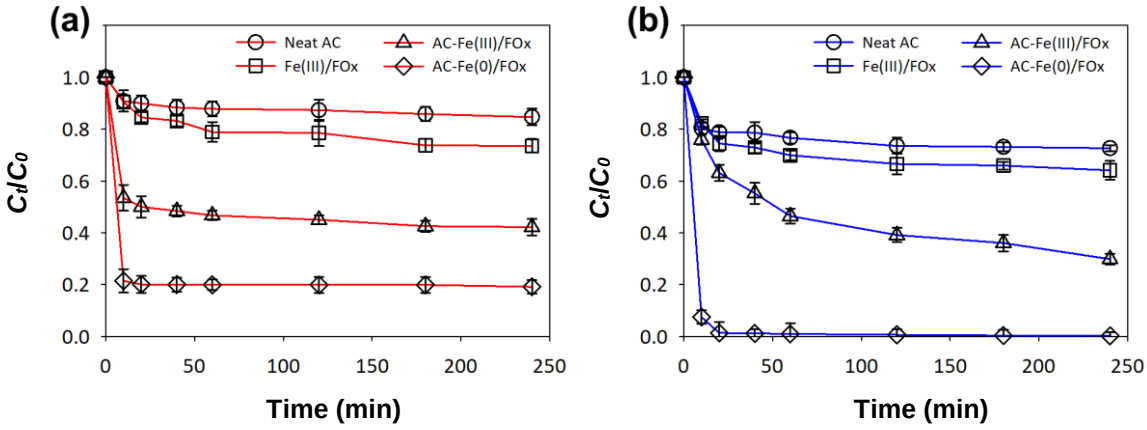

Fig. 4. Degradation kinetics of: (a) ASL and (b) furfural by adsorption, oxidation, and integration adsorption-oxidation (Fenton's reagents: 8 mg/L; H_2O_2: 200 mmol; pH: 5; ASL: 100%; furfural: 1000 mg/L)

The reactivity of Fe(0) is slightly different with the typical iron-base Fenton's reagent. Without the oxidation agent, the possible reaction of Fe(0) is described in Eqs. 11 to 13 below (Flores *et al*. 2008).

$$Fe^0+R+H^+ \rightarrow Fe^{2+}+RH \quad (11)$$

$$2Fe^{2+}+4H^++O_2+2H_2O \rightarrow 2Fe^{3+}+2H_2O \quad (12)$$

$$2Fe^{2+}+2H_2O \rightarrow 2Fe^{3+}+H_2+2OH^- \quad (13)$$

In addition, the integration of adsorption-oxidation with in situ formation of Fe(0) on the AC (AC-Fe(0)/FOx) was more favorable for the removal of ASL and furfural. As AC-Fe(0)/FOx immersed in the effluent, the degradation of ASL and furfural was able to achieve at 80.9 and 99.2% in the short times.

To observe the performance of the integration of adsorption-oxidation more clearly, the percentage of furfural removal was plotted in Fig. 5(a). The adsorption-oxidation kinetics at 1500 mg/L of furfural was plotted based on a pseudo-first-order relationship, using non-linear regression, where the coefficient of determination based on all samples was above ~0.98. The rates constant of furfural removal, *k* of AC-(III)/FOx was slightly lower in comparison with neat AC at 0.0197 and 0.0559 min^{-1}, respectively. Although the efficiency of AC-Fe(III)/FOx was considerably higher than neat AC, the integration of adsorption-oxidation provided a complex heterogenous reaction. Besides, the rates reaction in redox cycle of Fe(III) to Fe(II) in the primary reactions of the Fenton system are able to suppress the hydroxyl radical generation (Kent *et al*. 2015).

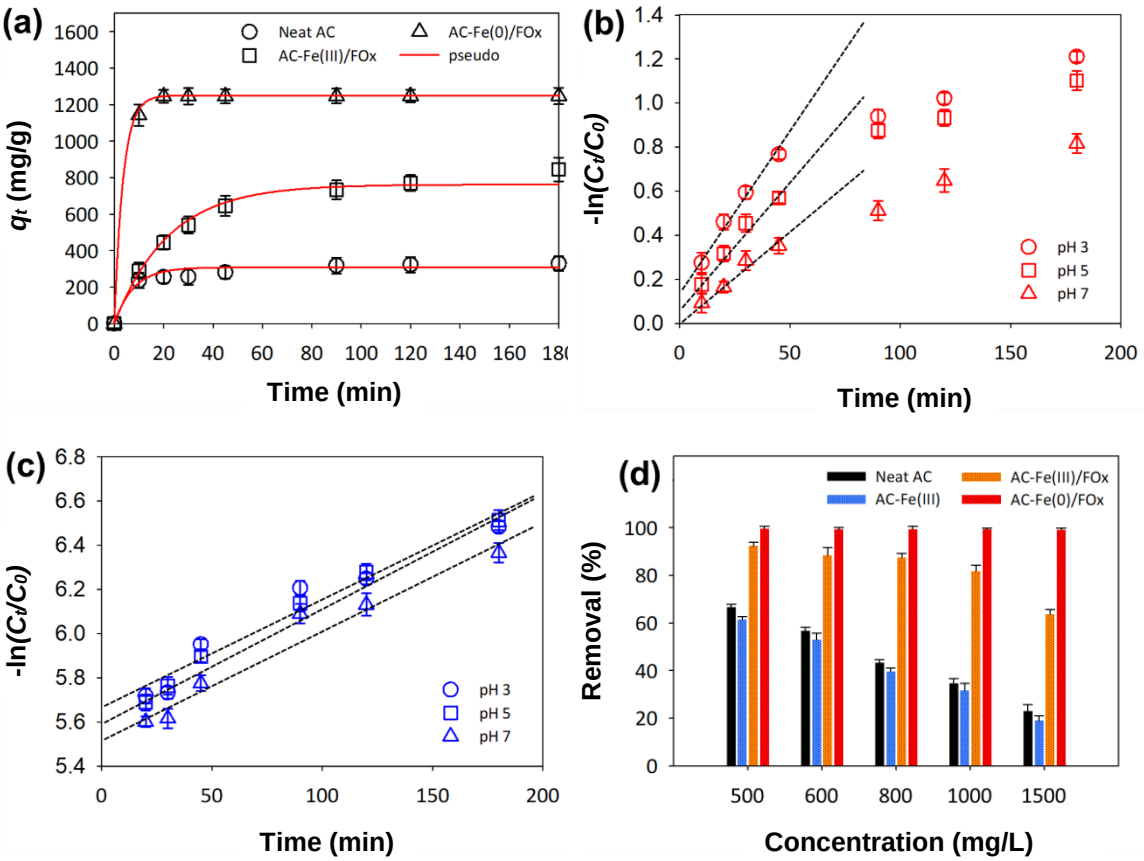

Fig. 5. Efficiency of furfural removal using adsorption-oxidation reaction fitted by: (a) non-linear regression of pseudo first order at pH 5, linear regression of Langmuir-Hinshelwood at different pH of (b) AC-Fe(III)/FOx, (c) AC-Fe(0)/FOx, and (d) the effect of different initial concentrations of furfural at pH 5 (adsorbent: 0.1 g; H_2O_2: 200 mmol; pH: 3-7; furfural: 500-1500 mg/L)

The mechanism of adsorption-oxidation of furfural by AC-Fe(III)/FOx and AC-Fe(0)/FOx could be described by Langmuir-Hinshelwood (LH) kinetics in terms of $-ln(C_0/C_t)$ over reaction time [see Fig. 5(b) and Fig. 5(c)] (Islam *et al*. 2016). Based on the pseudo-first-order rate constant, *k*, the rate of degradation of furfural by AC-Fe(III)/FOx was about 0.0167 min^{-1} in the initial 30 min of the reaction. This later underwent a significant reduction to about 0.122 min^{-1}. The rapid reaction of Fe(0) towards furfural degradation denoted with an incomparable performance since the *k*-value was significantly higher (0.1216 min^{-1}). Even though the low pH substantially improved the rate of removal of furfural, the deviations between the reaction rates were negligible (Duesterberg *et al*. 2008; Gholami *et al*. 2018).

On another note, even the highest initial concentration of furfural saw a significant improvement in the performance of AC-Fe(0)/FOx (Fig. 5d). On the contrary, the performance of AC-Fe(III)/FOx gradually declined at higher concentrations of furfural; at an initial concentration of 1,500 mg/L, the percentage removal of furfural was 63.8%. This occurrence was likely to be due to the ability of AC to uptake furfural of higher concentrations (Fig. 3b) apart from the insufficient oxidative activity.

CONCLUSIONS

1. Even though adsorption and catalytic oxidation had decent detoxification capacities, the integration of both techniques further improved the removal of target hydrolysate inhibitors. Specifically, the integrated technique had ASL and furfural removal rates two to three times those of the individual reactions [*i.e.* adsorption by activated carbon or catalytic oxidation by Fe(III)].
2. Additionally, the expeditious reaction of AC-Fe(0)/FOx removed 80.9% and 99.2% of ASL and furfural, respectively, within half an hour into the reaction. Evidently, the adsorptive-oxidative process could be enhanced by a good distribution of Fe(0) on the AC. Thus, the integration of the aforementioned techniques is likely to be beneficial for the pre-conditioning of lignocellulosic hydrolysate prior to bioconversion.

ACKNOWLEDGMENTS

The authors are grateful for the support of the Universiti Kebangsaan Malaysia, Grant No. DIP-2017-017 and GUP-2018-014.

REFERENCES CITED

Chaturvedi, V., and Verma, P. (2013). "An overview of key pretreatment processes employed for bioconversion of lignocellulosic biomass into biofuels and value added products," *3 Biotech* 3(5), 415-431. DOI: 10.1007/s13205-013-0167-8.

Chin, S. X., Chia, C. H., and Zakaria, S. (2013). "Production of reducing sugar from oil palm empty fruit bunch (EFB) cellulose fibres *via* acid hydrolysis," *BioResources* 8(1), 447-460. DOI: 10.15376/biores.8.1.447-460.

Chin, S. X., Tasirin, S. M., Chan, C. H., Chia, C. H., Chook, S. W., Zakaria, S., and Sajab, M. S. (2016). "Catalytic conversion of empty fruit bunch (EFB) fibres into lactic acid by lead (II) ions," *BioResources* 11(1), 2186-2201. DOI: 10.15376/biores.11.1.2186-2201.

Dantas, T. L. P., Mendonça, V. P., José, H. J., Rodrigues, A. E., and Moreira, R. F. P. M. (2006). "Treatment of textile wastewater by heterogeneous Fenton process using a new composite Fe_2O_3/carbon," *Chem. Eng. J*. 118(1-2), 77-82. DOI: 10.1016/j.cej.2006.01.016.

Duesterberg, C. K., Mylon, S. E., and Waite, T. D. (2008). "pH effects on iron-catalyzed oxidation using Fenton's reagent," *Environ. Sci. Technol*. 42(22), 8522-8527. DOI: 10.1021/es801720d.

Flores, Y., Flores, R., and Gallegos, A. A. (2008). "Heterogeneous catalysis in the Fenton-type system reactive black 5/H_2O_2," *J. Mol. Cataly. A-Chem*. 281(1-2), 184-191. DOI: 10.1016/j.molcata.2007.10.019.

Freundlich, H. (1907). "Over the adsorption in solution," *J. Phys. Chem*. 57(385471), 385-470. DOI: 10.1515/zpch-1907-5723.

Geng, B., Jin, Z., Li, T., and Qi, X. (2009). "Preparation of chitosan-stabilized Fe0 nanoparticles for removal of hexavalent chromium in water," *Sci. Total Environ*. 407(18), 4994-5000. DOI: 10.1016/j.scitotenv.2009.05.051.

Gholami, N., Ghasemi, B., Anvaripour, B., and Jorfi, S. (2018). "Enhanced photocatalytic degradation of furfural and a real wastewater using UVC/TiO_2 nanoparticles immobilized on white concrete in a fixed-bed reactor," *J. Ind. Eng. Chem*. 62, 291-301. DOI:10.1016/j.jiec.2018.01.007.

Gould, J. M. (1985). "Studies on the mechanism of alkaline peroxide delignification of agricultural residues," *Biotechnol. Bioeng*. 27(3), 225-231. DOI: 10.1002/bit.260270303.

Islam, M. T., Padilla, J. E., Dominguez, N., Alvarado, D. C., Alam, M. S., Cooke, P., Tecklenburg, M. M. J., and Noveron, J. C. (2016). "Green synthesis of gold nanoparticles reduced and stabilized by squaric acid and supported on cellulose fibers for the catalytic reduction of 4-nitrophenol in water," *RSC Adv*. 6(94), 91185-91191. DOI: 10.1039/C6RA17480A.

Jönsson, L. J., and Martín, C. (2016). "Pretreatment of lignocellulose: Formation of inhibitory by-products and strategies for minimizing their effects," *Bioresource Technol*. 199, 103-112. DOI: 10.1016/j.biortech.2015.10.009.

Kent, M. S., Avina, I. C., Rader, N., Busse, M. L., George, A., Sathitsuksanoh, N., Baidoo, E., Timlin, J., Giron, N. H., Celina, M. C., and Martin, L. E. (2015). "Assay for lignin breakdown based on lignin films: insights into the Fenton reaction with insoluble lignin," *Green Chem*. 17(10), 4830-4845. DOI: 10.1039/C5GC01083G.

Langmuir, I. (1917). "The constitution and fundamental properties of solids and liquids," *J. Am. Chem. Soc*. 38(11), 2221-2295. DOI: 10.1016/S0016-0032(17)90938-X.

Minella, M., Marchetti, G., De Laurentiis, E., Malandrino, M., Maurino, V., Minero, C., Vione, D., and Hanna, K. (2014). "Photo-Fenton oxidation of phenol with magnetite as iron source," *Appl. Catal. B-Environ*. 154, 102-109. DOI: 10.1016/j.apcatb.2014.02.006.

Mishima, D., Tateda, M., Ike, M., and Fujita, M. (2006). "Comparative study on chemical pretreatments to accelerate enzymatic hydrolysis of aquatic macrophyte biomass used in water purification processes," *Bioresource Technol*. 97(16), 2166-2172. DOI: 10.1016/j.biortech.2005.09.029.

Onganer, Y., and Temur, Ç. (1998). "Adsorption dynamics of Fe(III) from aqueous solutions onto activated carbon," *J. Colloid. Interf. Sci*. 205(2), 241-244. DOI: 10.1006/jcis.1998.5616.

Oruç, Z., Ergüt, M., Uzunoğlu, D., and Özer, A. (2019). "Green synthesis of biomass-derived activated carbon/Fe-Zn bimetallic nanoparticles from lemon (*Citrus limon* (L.) Burm. f.) wastes for heterogeneous fenton-like decolorization of Reactive Red 2," *J. Environ. Chem. Eng*. 103231, 1-10. DOI: 10.1016/j.jece.2019.103231.

Pereira, M. C., Oliveira, L. C. A., and Murad, E. (2012). "Iron oxide catalysts, Fenton and Fentonlike reactions: A review," *Clay Miner*. 47(3), 285-302. DOI: 10.1180/claymin.2012.047.3.01.

Phenrat, T., and Saleh, N. (2007). "Aggregation and sedimentation of aqueous nanoscale zerovalent iron dispersions," *Environ. Sci. Technol*. 41(1), 284-290. DOI: 10.1021/es061349a.

Qureshi, N., and Manderson, G. J. (1995). "Bioconversion of renewable resources into ethanol: An economic evaluation of selected hydrolysis, fermentation, and membrane technologies," *Energ. Source* 17(2), 241-265. DOI: 10.1080/00908319508946081.

Rosická, D., and Sembera, J. (2011). "Influence of structure of iron nanoparticles in aggregates on their magnetic properties," *Nanoscale. Res. Lett*. 6(1), 527. DOI: 10.1186/1556-276X-6-527.

Saad, M. J., Chia, C. H., Zakaria, S., Sajab, M. S., Misran, S., Rahman, M. A. A., and Chin, S. X. (2019). "Physical and chemical properties of the rice straw activated carbon produced from carbonization and KOH activation processes," *Sains Malays*. 48(2), 385-391. DOI: 10.17576/jsm-2019-4802-16.

Sajab, M. S., Ismail, N. N. N., Santanaraj, J., Mohammad, A. W., Hassan, H. A., Chia, C. H., Zakaria, S., and Noor, A. A. M. (2019). "Insight observation into rapid discoloration of batik textile effluent by in situ formations of zero valent iron," *Sains Malays*. 48(2), 393-399. DOI: 10.17576/jsm-2019-4802-17.

Sambusiti, C., Monlau, F., Antoniou, N., Zabaniotou, A., and Barakat, A. (2016). "Simultaneous detoxification and bioethanol fermentation of furans-rich synthetic hydrolysate by digestate-based pyrochar," *J. Environ. Manage*. 183, 1026-1031. DOI: 10.1016/j.jenvman.2016.09.062.

Santanaraj, J., Sajab, M. S., Mohammad, A. W., Harun, S., Chia, C. H., Zakari, S., and Kaco, H. (2017). "Enhanced delignification of oil palm empty fruit bunch fibers with in situ Fenton-oxidation," *BioResources* 12(3), 5223-5235. DOI: 10.15376/biores.12.3.5223-5235.

Santos, F. S. D., Lago, F. R., Yokoyama, L., and Fonseca, F. V. (2017). "Synthesis and characterization of zero-valent iron nanoparticles supported on SBA-15," *J. Mater. Res. Technol*. 6(2), 178-183. DOI: 10.1016/j.jmrt.2016.11.004.

Shi, S., Zhou, X., Chen, W., Chen, M., Nguyen, T., Wang, X., and Zhang, W. (2017). "Improvement of structure and electrical conductivity of activated carbon by catalytic graphitization using N_2 plasma pretreatment and iron (III) loading," *RSC Adv*. 7(71), 44632-44638. DOI: 10.1039/C7RA07328C.

Soleimani, M., Tabil, L., and Niu, C. (2015). "Adsorptive isotherms and removal of microbial inhibitors in a bio-based hydrolysate for xylitol production," *Chem. Eng. Commun*. 202(6), 787-798. DOI: 10.1080/00986445.2013.867258.

Suh, J., Zhu, B. Z., and Frei, B. (2003). "Ascorbate does not act as a pro-oxidant towards lipids and proteins in human plasma exposed to redox-active transition metal ions and hydrogen peroxide," *Free Radical Bio. Med*. 34(10), 1306-1314, DOI: 10.1016/S0891-5849(03)00147-3.

Sun, Y. P., Li, X. Q., Cao, J., Zhang, W. X., and Wang, H. P. (2006). "Characterization of zero-valent iron nanoparticles," *Adv. Colloid. Interfac*. 120(1-3), 47-56. DOI: 10.1016/j.cis.2006.03.001.

Torrey, J. D., Killgore, J. P., Bedford, N. M., and Greenlee, L. F. (2015). "Oxidation behavior of zero-valent iron nanoparticles in mixed matrix water purification membranes," *Environ Sci-Wat. Res*. 1(2), 146-152. DOI: 10.1039/C4EW00068D.

Yan, W., Herzing, A. A., Kiely, C. J., Zhang, W. X. (2010). "Nanoscale zero-valent iron (nZVI): Aspects of the core-shell structure and reactions with inorganic species in water," *J. Contam. Hydrol*. 118(3-4), 96-104. DOI: 10.1016/j.jconhyd.2010.09.003.

Zhang, Y., Su, Y., Zhou, X., Dai, C., and Keller, A. A. (2013). "A new insight on the core-shell structure of zerovalent iron nanoparticles and its application for Pb(II) sequestration," *J. Hazard. Mater*. 263, 685-693. DOI: 10.1016/j.jhazmat.2013.10.031.

Zhang, Z., Wang, X., Zhao, M., and Qi, H. (2014). "Free-radical degradation by Fe^{2+}/Vc/H_2O_2 and antioxidant activity of polysaccharide from *Tremella fuciformis*," *Carbohyd. Polym.* 112, 578-582. DOI: 10.1016/j.carbpol.2014.06.030.

Article submitted: July 16, 2019; Peer review completed: Peer review completed: September 3, 2019; Revised version received: September 13, 2019; Accepted: September 10, 2019; Published: September 17, 2019.
DOI: 10.15376/biores.14.4.8614-8626